Check for updates

Advanced Theory and Simulations

ADVANCED THEORY AND SIMULATIONS
www.advtheorysimul.com

RESEARCH ARTICLE OPEN ACCESS

In Silico Study of Degradation in Host Molecular Materials for OLEDs

Prashant Kumar[1,3] | Chen Zhou[2,4] | Pascal Friederich[2,4] | Daniel Escudero[3]

[1]Department of Chemistry, University College London, London, UK | [2]Institute of Nanotechnology, Karlsruhe Institute of Technology, Karlsruhe, Germany | [3]Quantum Chemistry and Physical Chemistry Division, Department of Chemistry, KU Leuven, Celestijnenlaan 200F, Leuven, Belgium | [4]Institute of Theoretical Informatics, Karlsruhe Institute of Technology, Karlsruhe, Germany

Correspondence: Prashant Kumar (prashant.kumar@ucl.ac.uk) | Daniel Escudero (daniel.escudero@kuleuven.be)

Received: 26 June 2026 | **Revised:** 18 September 2026 | **Accepted:** 8 October 2026

Keywords: OLEDs | degradation | DFT | molecular dynamics | machine learning

ABSTRACT

We investigate degradation in three OLED host materials: TBSO (4-(m-tolylsulfonyl)-1,1-biphenyl), DPPCarba (9-(3,5-diphenylphenyl)carbazole), and DPPTriphen (2-(3,5-diphenylphenyl)triphenylene), using static electronic-structure calculations, non-adiabatic molecular dynamics (NAMD), and machine-learning-accelerated NAMD (ML-NAMD). Static analysis identifies DPPTriphen as having the most favorable overall stability profile, whereas TBSO shows the greatest degradation susceptibility, with S–aryl cleavage emerging as an important pathway. All three hosts are also vulnerable under high-energy exciton–exciton annihilation conditions. Direct NAMD shows that TBSO can undergo bond dissociation on a sub-picosecond timescale. A fully connected neural-network potential reproduces the reference data with $R^2 = 0.999$ for energies and $R^2 = 0.998$ for forces, while providing an approximately 4.2×10^3 speedup over direct NAMD. This enables 3519 trajectories to be propagated to 1 ps and yields 29 degradation events from the first excited state. These results show that static descriptors alone do not fully capture degradation propensity and that explicit excited-state dynamics provides complementary mechanistic insight for designing more stable OLED host materials.

1 | Introduction

The development of organic light-emitting diodes (OLEDs) has transformed the landscape of display and lighting technologies. In 1987, Tang and VanSlyke published groundbreaking work on small-molecule-based OLEDs [1], and in 1990, Friend et al. first described polymer-based OLEDs [2]. Since then, the technology of OLEDs has attracted both industrial and academic interest [3–5]. Over the years, multiple generations of OLED emitters have been developed. The first [1], second [6], and third [7] generations of OLEDs are based on fluorescent, phosphorescent, and thermally activated delayed fluorescence (TADF) type of emitters, respectively, with the latter two achieving internal quantum efficiencies (IQEs) approaching unity. More recently, advanced concepts such as Hyperfluorescence [8], direct singlet harvesting (DSH) mechanisms [9], and inverted singlet-triplet (INVEST) [10] mechanisms have also been proposed. These advancements in OLEDs lighting and display technologies have surpassed traditional light-emitting diode (LED) technologies in commercial applications, particularly in the realm of display [11, 12].

Although significant progress in the OLEDs industry has been made by leaps and bounds, a key concern of the low operational stability of materials in OLEDs remains a challenging issue in the field [13]. In particular, chemical degradation of the host materials in the emissive layer is regarded as one of the key factors limiting device lifetimes [14–16]. Ideal host materials must

This is an open access article under the terms of the Creative Commons Attribution License, which permits use, distribution and reproduction in any medium, provided the original work is properly cited.
© 2026 The Author(s). *Advanced Theory and Simulations* published by Wiley-VCH GmbH

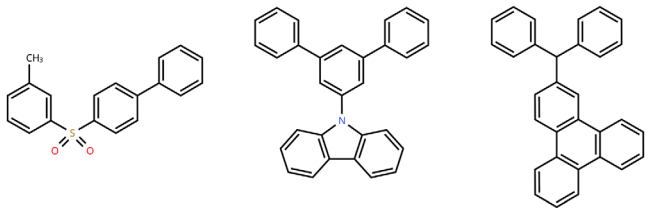


FIGURE 1 | Chemical structures of the OLED host molecules investigated in this study: TBSO, DPPCarba, and DPPTriphen.

exhibit ambipolar charge-transport properties while providing sufficiently high triplet energies (3 eV for blue OLEDs) to ensure efficient energy transfer to the dopant. The intrinsic chemical degradation in the host materials can occur through two mechanisms: an unimolecular one and a bimolecular one. Unimolecular degradation can be caused by inherent instabilities of the polarons or the excitons. Conversely, the bimolecular mechanisms are driven by annihilation processes between polarons and excitons. Among the latter, exciton–polaron annihilation (EPA) and exciton–exciton annihilation (EEA) are believed to be the dominant mechanisms responsible for chemical deterioration in OLEDs [17]. In its turn, EEA processes can be divided into singlet-singlet annihilation (SSA), singlet-triplet annihilation (STA) and triplet–triplet annihilation (TTA) depending on the spin symmetry of the involved excitons. For second- and third-generation OLEDs, where exciton lifetimes span the nanosecond to microsecond range, TTA is particularly prominent [17]. In OLED materials, TTA is usually the more relevant channel in a static stability analysis because triplet excitons have much longer lifetimes than singlet excitons and can therefore accumulate to higher steady-state concentrations. These annihilation processes can generate highly energetic excited states. In particular, TTA can populate higher-lying singlet states, S_n, when the energetic condition $2E(T_1) \geq E(S_n)$ is satisfied. In blue OLED materials, where triplet energies are commonly of the order of 3 eV, higher-lying singlet states with energies approaching 6 eV may therefore become energetically accessible [18]. Such energies substantially exceed the dissociation energies of many common covalent bonds and may consequently open degradation pathways that are inaccessible from the lowest excited state, such as the average bond energies of C–H, C–C, C–N, and C–S bonds being 4.28, 3.60, 3.16, and 2.68 eV, respectively [19]. Moreover, EPA and EEA processes also quench photoluminescence by converting excitons back to the ground state, contributing to the efficiency roll-off commonly observed at high exciton densities [20]. Because these diffusion-driven processes occur on ultrafast timescales (femtoseconds to picoseconds) and become more prominent under high-brightness conditions, understanding their impact on the chemical stability of host molecules is essential for designing longer-lived OLEDs [21].

In this work, we present a comprehensive first-principles investigation into the chemical degradation mechanisms of three widely used OLED host materials–TBSO, DPPCarba, and DPPTriphen (as shown in Figure 1) [22, 23]. To identify thermodynamically susceptible sites, we first computed bond dissociation energies (BDEs) for all potentially cleavable C–C, C–N, and C–S bonds in the above-mentioned host molecules, using a highly accurate double hybrid DFT functional (B2PLYP) for ground-state energetics and the algebraic diagrammatic construction scheme of second order (ADC(2)) for excited-state energies. Although these static calculations provide valuable insight into the thermodynamic driving forces of bond cleavage in the ground state, the first excited state, and the high-energy states generated via EEA and EPA, they inherently neglect the dynamical aspects of bond-breaking processes. Taking into account the shortcomings of using the above-described static approach, which only considers thermodynamic aspects. We performed nonadiabatic molecular dynamics (NAMD) simulations employing the fewest switches surface hopping (FSSH) algorithm to probe excited-state deactivation dynamics and kinetic pathways for chemical degradation over a 1 ps timescale with a 0.5 fs timestep. Given the computational cost of standard NAMD and the stochastic nature of bond dissociation events, we also used machine learning accelerated NAMD (ML-NAMD) simulations to speed up reaction discovery, particularly for TBSO, by efficiently generating a larger number of trajectories, thereby enhancing the statistical significance of our analysis. By integrating static calculations with dynamical simulations, we provide a molecular-level understanding of the degradation mechanisms in OLED host molecules. The novel findings of this study will help to design next-generation OLEDs materials with improved operational stability.

2 | Computational Details

2.1 | Optimization and Hessian

The ground-state and charged-state geometry optimization and hessian calculations were performed with density functional theory (DFT) [24, 25] with hybrid functional B3LYP [26–28] in combination with 6-31G* basis set [29, 30] for all the atoms. For the optimization of excited states, time-dependent DFT (TD-DFT) [31–34] with the same level of theory as in the ground-state calculations was used with the Gaussian 16 package [35].

2.2 | Bond Dissociation Energy

The BDEs of the host molecules were computed only for the homolytic fission with the Equation (1):

$$\mathrm{BDE} = E_{\mathrm{AB}} - (E_{\mathrm{A}} + E_{\mathrm{B}}) \tag{1}$$

For the single point calculations to calculate BDEs we have used the double hybrid DFT functional B2PLYP in combination with 6-311G* basis set for all atoms [36]. The Gaussian 16 package was used for this purpose.

2.3 | Excitation Energy

For the accurate adiabatic and Frank–Condon excitation energy, the algebraic diagrammatic construction scheme of second order (ADC(2)) [37–40] in combination with the def2-TZVP basis set [41] for all the atoms was used with the Turbomole 7.0 package [42].

25130390, 2026, 10, Downloaded from https://advanced.onlinelibrary.wiley.com/doi/10.1002/adts.70584 by Karlsruher Institut Fur Technologie, Wiley Online Library on [02/11/2026]. See the Terms and Conditions (https://onlinelibrary.wiley.com/terms-and-conditions) on Wiley Online Library for rules of use; OA articles are governed by the applicable Creative Commons License

2.4 | Molecular Dynamics (MD)

Fewest Switches Surface Hopping (FSSH) was used to investigate degradation from a dynamical perspective. FSSH is a mixed quantum–classical method in which an ensemble of independent trajectories approximates nuclear wave-packet motion, with each trajectory propagated on one electronic state at a time [43–45]. Transitions between electronic states are treated stochastically using Tully's fewest-switches algorithm, which minimizes the number of hops while preserving the electronic-state populations [46]. We conducted simulations of the FSSH dynamics in two distinct scenarios. First, we initiated the simulations from the S_1 state to assess the stability of the molecule in its first excited state. Second, we initiated the simulations from the S_6 state to examine the stability of the molecule in the SSA process, for TBSO, the S_6 state lies at 5.95 eV and was therefore chosen as a representative high-energy initial state. To ensure a comprehensive analysis, we generated a total of 100 trajectories for the scenario when starting from S_1 and 50 trajectories for the scenario when starting from S_6. The initial conditions, i.e., position and momentum, were generated using the Wigner distribution for the quantum harmonic oscillator. Each trajectory was simulated for a duration of 1 picosecond, employing a time step of 0.5 femtoseconds. To obtain the necessary energy and gradient values, we employed the TD-B3LYP method in combination with the def2-SV(P) basis set. The nonadiabatic couplings (NACs) in Newton-X 2.2 were evaluated as time-derivative couplings from wavefunction overlaps between electronic states at consecutive nuclear time steps, using the local-diabatic representation [47, 48]. Within the present TDDFT-based dynamics setup, transitions from S_1 to S_0 were not included because the required ground-state–excited-state NACs are not available in the same way as excited-state–excited-state couplings in the standard linear-response TDDFT framework [49]. For these computations, we utilized the NewtonX 2.2 [50] and Turbomole 7.0 packages [42].

2.5 | Machine Learning

As our use case aims at high accuracy and speed, rather than generalizability to other molecules, we use a fully connected neural network (NN) inspired by prior work for simulations of TBSO [51, 52]. The NN is trained to predict energies E_i and forces F_i using a combined mean squared error loss function ℓ, with forces trained as negative gradients of energies w.r.t. the atom positions R_i (Equation 2). We incorporate a masking mechanism in the loss function that leaves out missing labels during the training process to handle missing energy and force labels resulting from changes in electronic states. The NN takes as input an inverse distance-based feature representation of TBSO, which consists of 703 features resulting from $N = 38$ atoms. There are 7 electronic states (ground state and 6 excited states; $k = 7$) that lead to 7 energy values and $k \times 3N = 798$ gradient components as the model outputs. The NN models consist of 6 layers with 5000 neurons per layer and a sharp-softplus activation function (See Section S1). The training process is carried out with the Adam optimizer, a DFT-calculated data set from the static analyzes that is randomly split for training (70 815 data points) and testing (23 604 data points), and an exponential decrease of learning rate from 10^{-6} over 1000 epochs. The NN models were implemented using TensorFlow/Keras (v2.10) (see Supporting Information for hyperparameter tuning and ML training details).

TABLE 1 | ADC(2) vertical and adiabatic excitation energies of the first excited singlet and triplet states for the three host molecules. In the main text, E_{S_1} and E_{T_1} refer to the adiabatic S_1 and T_1 excitation energies, respectively. All energies are given in eV.

	S_1		T_1	
Molecule	**Vertical**	**Adiabatic**	**Vertical**	**Adiabatic**
TBSO	4.81	4.45	3.72	3.18
DPPCarba	3.94	3.74	3.61	3.40
DPPTriphen	3.98	3.80	3.32	2.97

$$\ell((\hat{E}_1,\ldots,\hat{E}_n),(E_1,\ldots,E_n,F_1,\ldots,F_n)) = \sum_{i=1}^{n} ||E_i - \hat{E}_i||^2 + \sum_{i=1}^{n} ||F_i - (-\frac{\partial \hat{E}_i}{\partial R_i})||^2 \quad (2)$$

For ML-NAMD simulations, we applied Zhu–Nakamura theory of surface hopping (ZNSH) [53] instead of the FSSH as the non-adiabatic couplings are challenging for ML prediction [52, 54]. ZNSH estimates the probability of surface hopping based on energies only and has been successfully applied to excited-state dynamics studies. To enhance the simulation efficiency, we incorporated PyRAI2MD [52] instead of NewtonX with NN potentials since this package is designed to readily utilize the NN predictions with a minimal number of I/O operations.

3 | Results and Discussion

The main goal of this work is to understand both the thermodynamic driving factors and the dynamical pathways leading to bond cleavage and thus degradation. In this section, we begin by examining the BDEs of all chemically susceptible bonds, establishing a thermodynamic baseline for molecular stability on the ground state and excited states. Then we move on to NAMD simulations to capture the dynamics underlying these degradation pathways, enabling a dynamic perspective that complements the static energy analysis. Finally, we employ ML-NAMD to improve the statistical robustness of our trajectory sampling in NAMD, allowing us to construct a comprehensive mechanistic picture of degradation in these host materials.

3.1 | Thermodynamic Stability and Bond Dissociation Energies

For the static BDE analysis, we use descriptors of stability for unimolecular dissociation (formation of exciton and polaron) and bimolecular dissociation (EPA and TTA, suggested by Freidzon et al. [22]). In Figure S6, we show how the adiabatic and vertical energies were computed. The computed ADC(2) excitation energies are shown in Table 1.

An OLED device is considered stable if, at 70°C, one-half of the initial luminance is not lost before 10^6 h of operation [17]. Using the Arrhenius equation, this lifetime criterion gives an

25130390, 2026, 10, Downloaded from https://advanced.onlinelibrary.wiley.com/doi/10.1002/adts.70584 by Karlsruher Institut Fur Technologie, Wiley Online Library on [02/11/2026]. See the Terms and Conditions (https://onlinelibrary.wiley.com/terms-and-conditions) on Wiley Online Library for rules of use; OA articles are governed by the applicable Creative Commons License

approximate energetic stability descriptor of $E_{charge} \approx 1.5$ eV for degradation processes occurring in charged molecular states. Therefore, for a molecule to be stable against degradation induced by hole or electron transport through the layer, the lowest bond dissociation energy in the cationic or anionic state should exceed 1.5 eV. For degradation in the first excited state, the relevant descriptor is defined as $\Delta E_{exc} = BDE_{GS} - E_{S1/T1}$, where BDE_{GS} is the ground-state bond dissociation energy and $E_{S1/T1}$ is the adiabatic excitation energy of the corresponding singlet or triplet state. In this case, the molecule is considered stable when ΔE_{exc} is larger than 1.4 eV for singlet excitons and 1.5 eV for triplet excitons [55].

This estimate also highlights the intrinsic difficulty of designing stable deep-blue phosphorescent molecules. Since blue phosphorescent emitters typically require triplet energies of approximately 3 eV, maintaining a residual stability margin of $\Delta E_{T1} = 1.5$ eV would require ground-state BDEs of roughly 4.5 eV. Such high BDEs are difficult to achieve for many bonds in organic molecules, making blue emitters particularly susceptible to excited-state degradation [56]. In addition to direct exciton-induced bond cleavage, degradation can also occur through exciton–polaron annihilation (EPA), also known as the hot-molecule dissociation mechanism. In this process, annihilation involving charged and excited species can generate a highly energetic molecular state that may dissociate if sufficient energy is available [57]. Therefore, we define the EPA stability descriptor as $\Delta E_{EPA} = BDE^{+/-} - E_{S1/T1}$, where $BDE^{+/-}$ is the BDE in the cationic or anionic state. To avoid spontaneous bond cleavage through EPA, ΔE_{EPA} should be positive [58]. Consequently, for blue phosphorescent molecules, the BDEs in the charged state should be larger than the relevant triplet excitation energy.

For exciton–exciton annihilation (EEA), also referred to as the highly excited-state dissociation mechanism, two excitons interact such that their excitation energies are combined on one molecule. Depending on the nature of the interacting excitons, this process can be described as SSA or STA or TTA. The corresponding stability descriptor is defined as $\Delta E_{EEA} = BDE_{GS} - 2E_{S_1/T_1}$, where the factor of two accounts for the energy of the two annihilating excitons. A positive value of ΔE_{EEA} indicates that the energy released by the annihilation process is insufficient to cleave the bond, while a negative value suggests that bond dissociation is energetically accessible [59]. For the TTA channel, the descriptor becomes $\Delta E_{TTA} = BDE_{GS} - 2E_{T_1}$. To suppress TTA-induced dissociation in blue phosphorescent molecules through TTA, ΔE_{TTA} should always be positive. In other words, the ground-state BDEs should therefore exceed twice the first triplet excited-state energy.

Using the degradation descriptors defined above, we compare the unimolecular stability of the three host molecules with respect to charge and exciton induced bond cleavage. The corresponding descriptors are shown in Figure 2, while the underlying BDEs are listed in Table S2 (more detailed information is given in Section S5). TBSO is predicted to be the least stable molecule, mainly because the S–aryl bonds are weak in the anionic state. In particular, Bond 1 and Bond 2 have BDE^- values of 1.00 and 1.10 eV, respectively, which are below the 1.5 eV charged-state stability threshold. TBSO is also unstable in the first excited singlet state, with Bond 1 giving $\Delta E_{S1} = -1.38$ eV. DPPCarba shows improved charged-state stability, although the anionic BDE of Bond 1 is slightly below the threshold at 1.39 eV. However, DPPCarba remains vulnerable to singlet-exciton-induced degradation, especially at Bond 1 (as shown in Figure S7), corresponding to the C–N bond, for which $\Delta E_{S1} = -0.37$ eV. In contrast, DPPTriphen shows the highest overall molecular stability against unimolecular degradation. All charged-state BDEs are well above the 1.5 eV threshold, and the excited-state descriptors are more favorable than those of TBSO and DPPCarba. Nevertheless, the singlet-state descriptor for Bond 2 remains below the required threshold, with $\Delta E_{S_1} = 0.79$ eV. Thus, although DPPTriphen is clearly the most robust of the three molecules considered here, singlet-exciton-induced degradation may still represent a possible limiting pathway. Overall, the unimolecular analysis follows the stability trend TBSO < DPPCarba < DPPTriphen.

For the bimolecular degradation pathways considered here include EPA and TTA. The corresponding static stability descriptors are shown in Figure 3. In this analysis, positive descriptor values indicate that the corresponding bond cleavage process is energetically unfavorable, whereas negative values indicate that dissociation is energetically accessible. All three molecules show negative ΔE_{TTA} values, suggesting that none of them is fully stable against TTA-induced degradation within the static picture. For the EPA process, DPPTriphen is predicted to be the most stable of the three molecules. All EPA descriptors for DPPTriphen are positive, indicating that bond cleavage through the considered EPA channels is energetically unfavorable. In contrast, TBSO and DPPCarba show several negative EPA descriptors. Between these two molecules, DPPCarba is comparatively more stable than TBSO. For DPPCarba, the most vulnerable EPA channel is the anionic singlet process at Bond 1, corresponding to the C–N bond, with $\Delta E_{EPA} = -2.35$ eV. For TBSO, the lowest EPA descriptor is obtained for Bond 1, corresponding to the S–aryl bond, with $\Delta E_{EPA} = -3.45$ eV. This indicates that TBSO is especially susceptible to EPA-induced cleavage in electron-rich excited configurations.

A general trend across the three molecules is that the anionic singlet EPA channel gives the lowest, and therefore least favorable, descriptor values among the exciton–polaron processes. This suggests that degradation following the interaction of an anionic species with a singlet exciton may be the most critical EPA pathway for these host molecules. Although DPPTriphen is stable with respect to the EPA descriptors, it remains unstable toward TTA-induced degradation. The lowest TTA descriptor for DPPTriphen is found for Bond 2, corresponding to the C–phenyl C bond, with $\Delta E_{TTA} = -1.35$ eV. Overall, the static bimolecular analysis gives the same stability trend as the unimolecular analysis, namely TBSO < DPPCarba < DPPTriphen. These results are consistent with previous multireference calculations by Freidzon et al. on DPPCarba and DPPTriphen [22].

3.2 | Excited-State Degradation Dynamics Using NAMD

The static degradation descriptors discussed above provide a useful energetic screening of the possible bond–cleavage pathways. However, these descriptors do not include the explicit time evolution of the nuclear geometry after excitation, nor do they

25130390, 2026, 10, Downloaded from https://advanced.onlinelibrary.wiley.com/doi/10.1002/adts.70584 by Karlsruher Institut Fur Technologie, Wiley Online Library on [02/11/2026]. See the Terms and Conditions (https://onlinelibrary.wiley.com/terms-and-conditions) on Wiley Online Library for rules of use; OA articles are governed by the applicable Creative Commons License

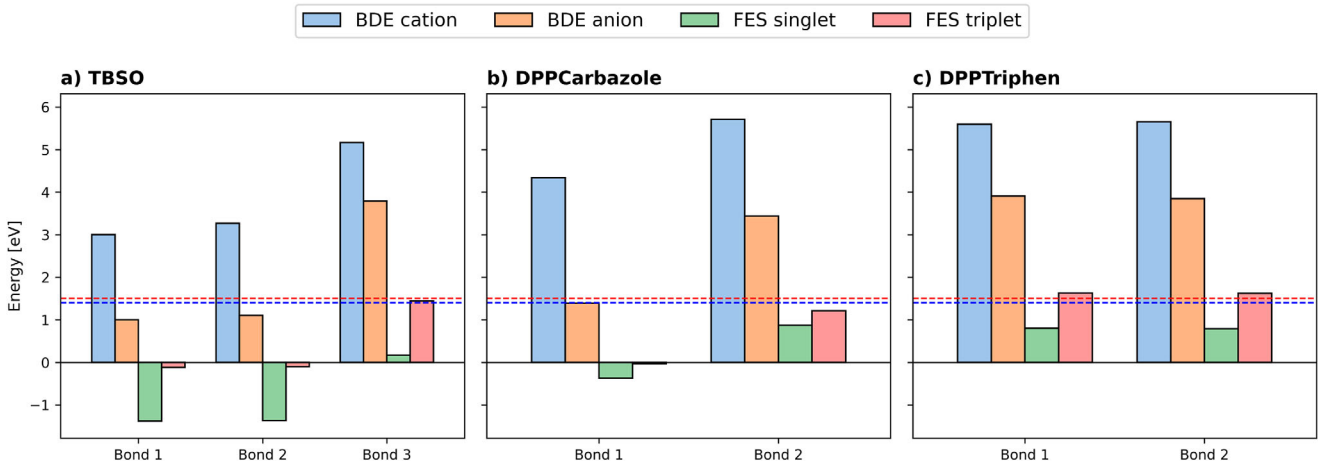


FIGURE 2 | Static analysis of unimolecular dissociation processes for (a) TBSO, (b) DPPCarba, and (c) DPPTriphen. The plotted quantities correspond to bond dissociation energies in the cationic and anionic states, together with the effective dissociation energies in the first excited singlet and triplet states. The red dashed horizontal line indicates the common 1.5 eV stability threshold used for charged-state and triplet-exciton-induced degradation, while the blue dashed horizontal line indicates the 1.4 eV threshold used for singlet-exciton-induced degradation.

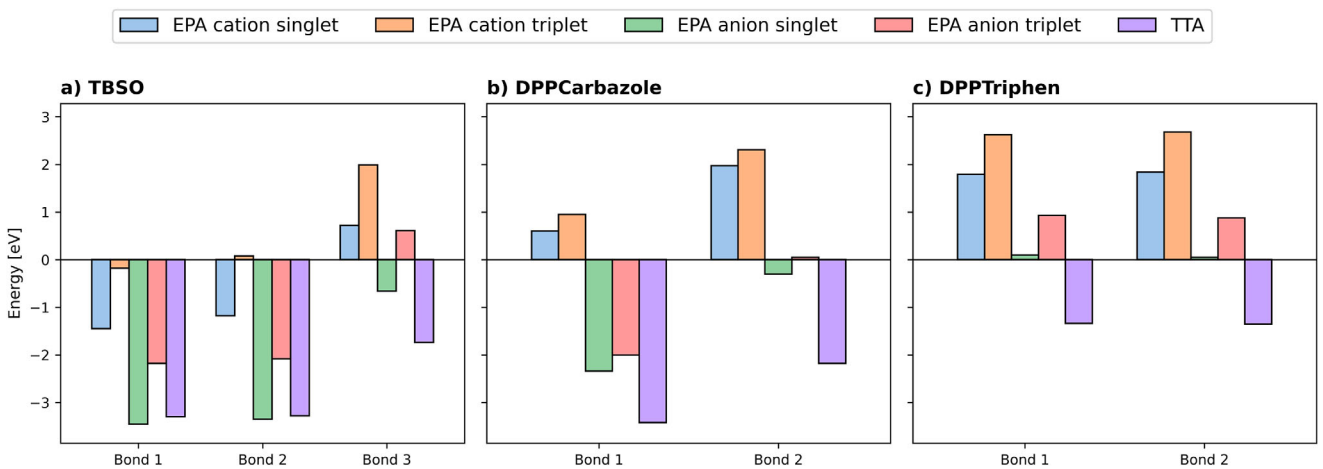


FIGURE 3 | Static analysis of bimolecular degradation processes for (a) TBSO, (b) DPPCarba, and (c) DPPTriphen. The plotted quantities correspond to the calculated stability descriptors for exciton–polaron annihilation in the cationic and anionic states and for triplet–triplet annihilation. Positive values indicate that the corresponding bond cleavage process is energetically unfavorable, whereas negative values indicate that dissociation is energetically accessible. The horizontal line at 0 eV therefore represents the stability threshold, above which the molecule is considered stable against the corresponding bimolecular degradation pathway.

show whether the weak bonds actually elongate or dissociate on a realistic timescale upon OLED operation. To gain further insight into the degradation dynamics, we therefore performed non-adiabatic excited-state dynamics simulations. Because such simulations are computationally demanding, especially for the large host molecules considered here, we selected TBSO as a representative system for the dynamics study. This choice is motivated by the static unimolecular and bimolecular analyzes, which identify TBSO as the least stable molecule among the three candidates. In particular, TBSO shows very low anionic BDEs for the S–aryl bonds and strongly negative excited-state stability descriptors, indicating a high probability of bond cleavage. Therefore, if dissociation is accessible within the short simulation time of approximately 1 ps, TBSO is expected to be the most likely candidate to show this behavior. In particular, TBSO shows weak S–aryl bonds in the anionic state and unfavorable excited-state stability descriptors, suggesting that it has the highest probability of exhibiting bond elongation or dissociation within the short simulation time accessible to direct dynamics. Therefore, fewest-switches surface hopping (FSSH) dynamics simulations were performed for TBSO over a time scale of 1 ps.

Two initial excitation scenarios were considered for the non-adiabatic dynamics simulations. In the first case, the trajectories were initialized in the S1 state to probe the stability of TBSO in the first excited singlet state. In the second case, the trajectories were initialized in the S_6 state to represent a high-energy excited-state conditions. Following TTA, a higher-lying singlet state, S_n, may be populated when $2E(T_1) \geq E(S_n)$. For blue OLED materials with triplet energies of the order of 3 eV, this criterion permits access

25130390, 2026, 10, Downloaded from https://advanced.onlinelibrary.wiley.com/doi/10.1002/adts.70584 by Karlsruher Institut Fur Technologie, Wiley Online Library on [02/11/2026]. See the Terms and Conditions (https://onlinelibrary.wiley.com/terms-and-conditions) on Wiley Online Library for rules of use; OA articles are governed by the applicable Creative Commons License

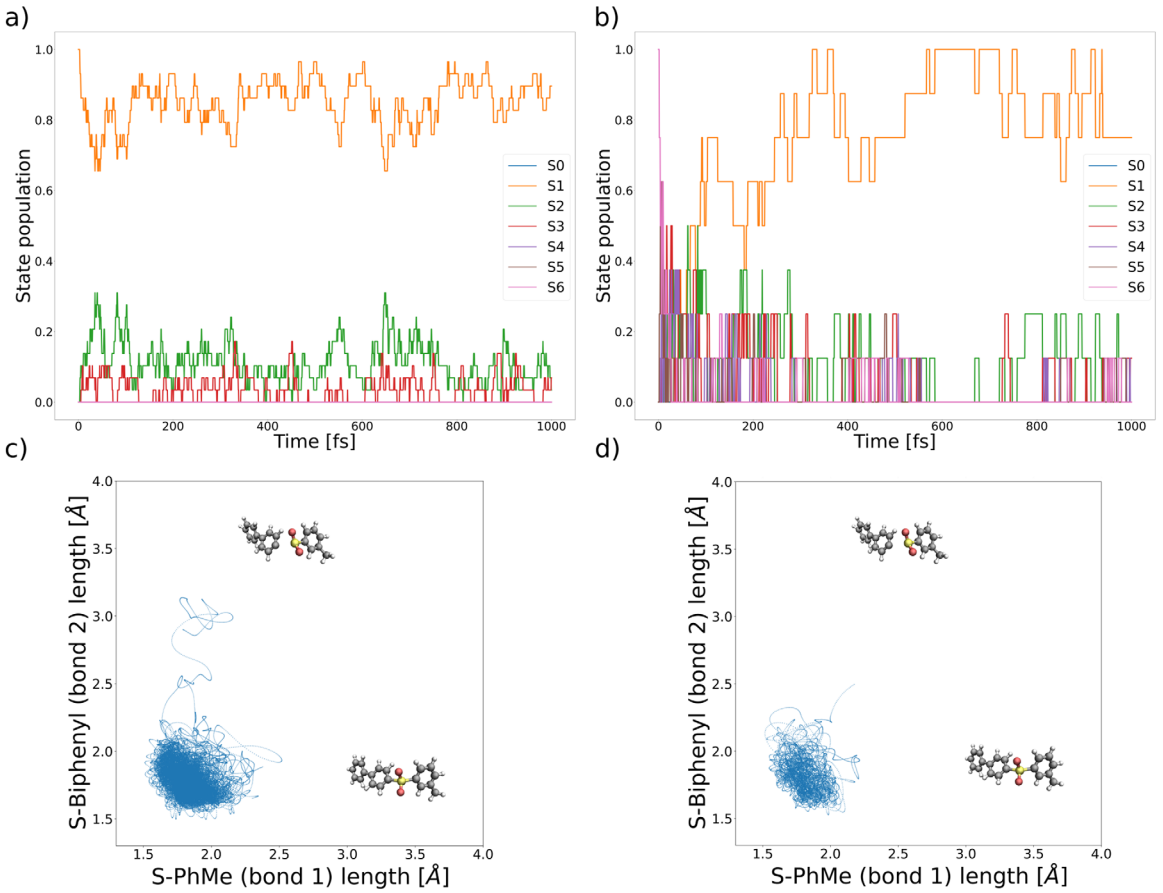


FIGURE 4 | FSSH dynamics of TBSO initialized from S_1 state and from S_6 state. State populations are shown for trajectories started from (a) S_1 and (b) S_6. Panels (c) and (d) show the corresponding time evolution of the two S–aryl bond lengths, Bond 1 and Bond 2, as S–C bond length distributions.

to singlet states with energies approaching 6 eV. The S_6 state of TBSO, with a vertical excitation energy of 5.95 eV, was therefore selected as a representative high-lying singlet state within this energy range. The simulations do not explicitly describe the bimolecular TTA process, nor is S_6 assumed to be its unique electronic product; instead, they probe the subsequent non-adiabatic dynamics and possible degradation following population of such a highly excited state.. Each trajectory was propagated for 1 ps using a time step of 0.5 fs. The initial conditions for the independent trajectories were generated from a harmonic Wigner distribution [60].

The resulting state populations and selected bond-length distributions are shown in Figure 4. When the dynamics is initiated from S_1, the population remains mainly on the low-lying excited states during the simulation, with S_1 being the dominant state throughout most of the trajectory time. In contrast, trajectories initialized from S_6 show rapid redistribution among several excited states, reflecting stronger non-adiabatic coupling and a more complex relaxation pathway from the higher excited-state manifold. The corresponding bond-length plots compare the evolution of Bond 1 and Bond 2, which correspond to the two S–aryl bonds identified as weak points in the static analysis. The sampled trajectories show occasional elongation of the S–biphenyl bond, i.e., Bond 2, suggesting that dissociation may preferentially proceed through this bond. However, within the limited number of completed 1 ps trajectories, the bond-length distributions of Bond 1 and Bond 2 remain broadly comparable, and no clear distinction between the two possible dissociation channels can be made from the direct FSSH simulations alone.

However, the direct FSSH simulations were limited by convergence problems. From the S_1 initial condition, 100 trajectories were started, but only 29 trajectories completed the full 1 ps simulation. For the S_6 initial condition, 50 trajectories were started, but only 8 trajectories reached 1 ps. The remaining trajectories terminated earlier because of electronic-structure convergence failures. Although all trajectories, including those that did not complete the full simulation time, were retained for training the machine-learning models discussed in the next section, the number of complete direct FSSH trajectories is not sufficient to draw statistically robust conclusions about the dissociation probability. Therefore, to obtain a more comprehensive dynamical picture and improve the statistical sampling, we next performed machine-learning-accelerated non-adiabatic dynamics simulations.

3.3 | Accuracy and Speed of the Trained ML Models

To benchmark the accuracy and speed of ML TBSO excited state potentials, we tested the trained NN model on the test set with 23 604 data points. The mean absolute error (MAE) and coefficient

25130390, 2026, 10, Downloaded from https://advanced.onlinelibrary.wiley.com/doi/10.1002/adts.70584 by Karlsruher Institut Fur Technologie, Wiley Online Library on [02/11/2026]. See the Terms and Conditions (https://onlinelibrary.wiley.com/terms-and-conditions) on Wiley Online Library for rules of use; OA articles are governed by the applicable Creative Commons License

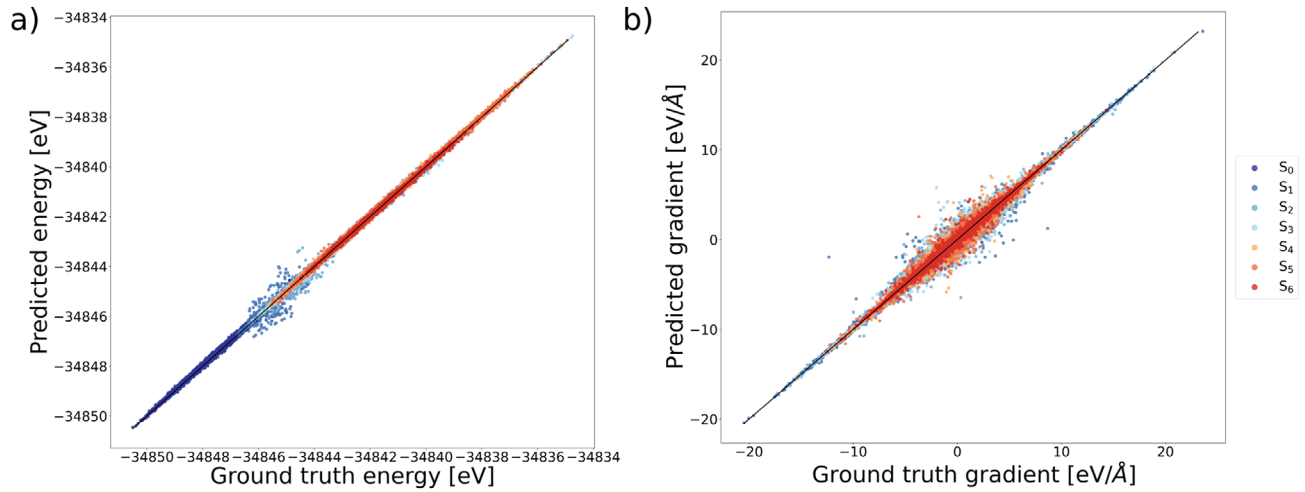


FIGURE 5 | Scatter plots of (a) energies and (b) gradients predicted by the NN model v.s. the TD-DFT ground truth value of all electronic states from S_0 to S_6. (a) The model achieves a MAE of 0.039eV and a R^2 value of 0.999. b) All gradient components of all atoms, in all three dimensions, and all electronic states are shown. The model achieves an overall MAE of 0.050eV · $Å^{-1}$ and a R^2 value of 0.998.

of determination (R^2) of the predicted energies and gradients are summarized in Figure 5. The NN model achieves the MAE of 0.039eV and R^2 of 0.999 on energy predictions, and the MAE of 0.050eV · $Å^{-1}$ and R^2 of 0.998 on gradient predictions, suggesting an almost linear correlation between NN predictions and DFT calculated labels.

The inference time (forward pass) of a single TBSO geometry in a single NN with 5000 neurons per layer to predict energies and forces takes 178.7ms on a single CPU. As a comparison, a TD-DFT (B3LYP/def2-SV(P)) calculation requires on average 754 s for a single molecular geometry. Neglecting the MD system update time, this comparison indicates a 4.2×10^3 acceleration of using a NN to propagate MD simulations compared to TD-DFT calculations. A further speedup can be obtained when using GPUs and parallelizing NN predictions over many molecular geometries in a batch-wise way: A forward pass of 89 geometries in parallel with the 5000 neurons per layer model on a GPU takes on average 51.4 ms (37.4 ms for a single geometry). With the ML accelerated simulation, we can collect 3519 ML-NAMD trajectories, each running over 1 picosecond, within 24 h.

3.4 | ML-NAMD Analysis

To assess the reliability of the trained machine-learning models during the dynamics simulations, the electronic-state populations obtained from direct NAMD and ML-NAMD simulations were compared. As shown in Figure 6, trajectories were initialized either from the first excited state (S_1) or from the sixth excited state (S_6). Owing to the much larger number of trajectories accessible with ML-NAMD, namely 3519 trajectories for S_1 and 2844 trajectories for S_6, the ML-NAMD state populations exhibit a much smoother time evolution than the corresponding direct NAMD results, which are based on only 29 and 8 completed trajectories for S_1 and S_6, respectively. Despite this difference in sampling, the overall population dynamics are comparable between the two approaches. In both cases, the population remains dominated by S_1 after the initial relaxation period, indicating that the ML model captures the main features of the excited-state relaxation. The remaining deviations between the ML-NAMD and direct NAMD populations can be attributed to the limited number of completed direct trajectories, as well as methodological differences between the ZNSH scheme used in ML-NAMD and the FSSH approach used in the direct NAMD simulations.

After validating the ML-NAMD state populations against the direct NAMD results, we used the larger ML-NAMD trajectory ensemble to analyze rare bond-elongation events associated with possible degradation.

The improved sampling enabled by ML-NAMD allows rare bond-elongation events to be identified within the 1 ps simulation window. For trajectories initialized from S_1, 29 out of 3519 ML-NAMD trajectories show abnormal elongation of Bond 2, defined here as an S–biphenyl bond length larger than 2.50 Å. This elongation is interpreted as a possible early signature of degradation or bond-cleavage initiation. As shown in Figure 7, the ML-NAMD results reproduce the same qualitative behavior observed in the direct NAMD simulations, where 1 out of 29 completed trajectories also shows abnormal elongation of Bond 2. The agreement between the direct and ML-accelerated simulations supports the conclusion that Bond 2 is a likely degradation-sensitive coordinate in TBSO. However, the much larger ML-NAMD trajectory ensemble provides a more statistically meaningful estimate of how frequently such bond-elongation events occur. Additional bond-length analyzes for trajectories initialized from S_6 and for the other selected bonds of TBSO are provided in the Supporting Information.

It is important to note that the static descriptors alone do not clearly distinguish between the two possible S–aryl dissociation pathways in TBSO. In the unimolecular analysis, both Bond 1 and Bond 2 show similarly unfavorable descriptors for first-excited-state stability, suggesting that either bond could act as a degradation site. A similar conclusion is obtained from the bimolecular static analysis, where the corresponding EPA and

25130390, 2026, 10, Downloaded from https://advanced.onlinelibrary.wiley.com/doi/10.1002/adts.70584 by Karlsruher Institut Fur Technologie, Wiley Online Library on [02/11/2026]. See the Terms and Conditions (https://onlinelibrary.wiley.com/terms-and-conditions) on Wiley Online Library for rules of use; OA articles are governed by the applicable Creative Commons License

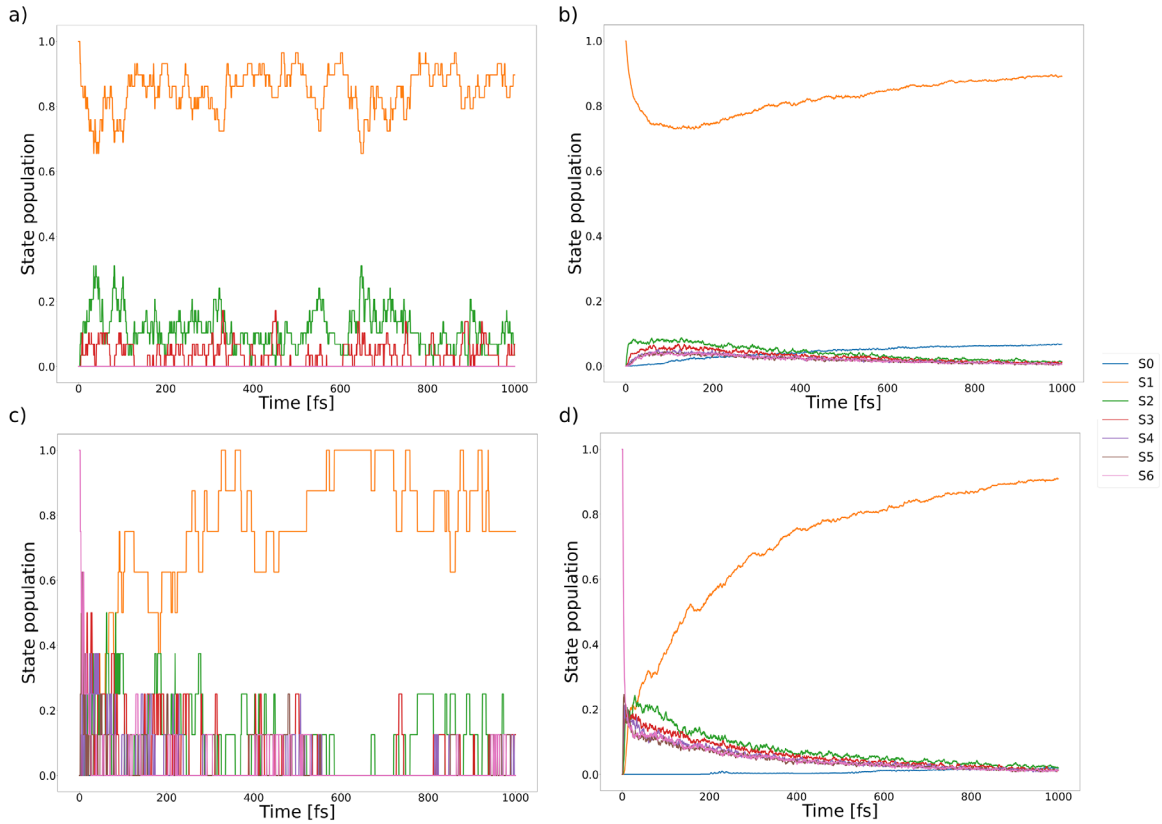


FIGURE 6 | Comparison of NAMD and ML-NAMD results on state populations during simulation. (a) NAMD trajectories initialized in the S_1 state. Populations average 29 trajectories. (b) ML-NAMD trajectories initialized at S_1. Populations average 3519 trajectories. (c) NAMD trajectories initialized at S_6. Populations average 8 trajectories. (d) ML-NAMD trajectories initialized at S_6. Populations average 2844 trajectories.

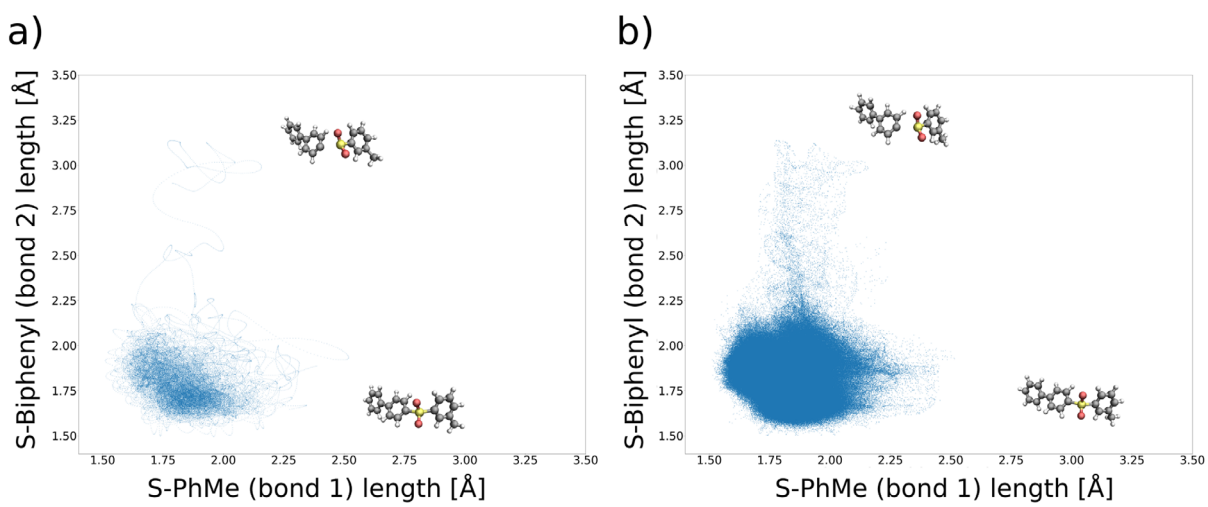


FIGURE 7 | Comparison of abnormal bond 2 lengths detected by NAMD and ML-NAMD for trajectories initialized at S_1. (a) 1 out of 29 trajectories with abnormal bond 2 lengths detected by NAMD. (b) 29 out of 3519 trajectories with abnormal bond 2 lengths detected by ML-NAMD.

TTA descriptors also indicate comparable instability for the two bonds. In contrast, the dynamics simulations provide a more detailed picture of the degradation process by explicitly following the time evolution of the molecular geometry. The ML-NAMD trajectories reveal that abnormal bond elongation occurs preferentially along Bond 2, indicating that this bond is more likely to initiate dissociation under the simulated conditions. This comparison highlights the importance of going beyond a purely static energetic picture when studying OLED degradation, since non-adiabatic dynamics can capture rare bond-elongation events and pathway preferences that are not evident from static descriptors alone [61, 62].

25130390, 2026, 10, Downloaded from https://advanced.onlinelibrary.wiley.com/doi/10.1002/adts.70584 by Karlsruher Institut Fur Technologie, Wiley Online Library on [02/11/2026]. See the Terms and Conditions (https://onlinelibrary.wiley.com/terms-and-conditions) on Wiley Online Library for rules of use; OA articles are governed by the applicable Creative Commons License

4 | Conclusions and Outlook

This work presents a comprehensive first-principles investigation of chemical degradation mechanisms in three classical OLED host materials: TBSO, DPPCarba, and DPPTriphen. By combining DFT/B2PLYP and ADC(2) calculations, we characterized the ground- and excited-state thermodynamics relevant to unimolecular and bimolecular degradation pathways. In addition, non-adiabatic molecular dynamics (NAMD) simulations to probe excited-state relaxation and degradation on the picosecond timescale. The static degradation descriptors show that DPPTriphen is the most robust candidate with respect to unimolecular dissociation and exciton–polaron annihilation (EPA), whereas TBSO is the least stable due to its weak S–aryl bond, making it unsuitable for general OLED applications. All three materials exhibit intrinsic susceptibility to degradation through triplet–triplet annihilation (TTA). Notably, the NAMD simulations further confirm that TBSO can undergo degradation on an ultrafast, sub-picosecond timescale.

To accelerate excited-state sampling, we trained a fully connected neural network for ML-NAMD, achieving a 4.2×10^3 speedup over standard NAMD while maintaining an $R^2 > 0.998$ for both energy and energy-gradient predictions. This acceleration enabled the generation of 3519 trajectories and the identification of 29 degradation events from the first excited state, which would be statistically inaccessible using conventional direct simulations alone. Current ML-NAMD is limited by its restricted performance on highly distorted geometries and near-crossing regions without sufficient NAMD training data, such as conformers with elongated S–C bonds. Future work will focus on expanding and refining the neural-network model to more fully represent the TBSO chemical space. In particular, we will employ parallel active learning [63] to efficiently enrich the dataset in under-sampled regions, especially those associated with dissociation events.

Author Contributions

P.K. contributed to methodology, investigation, data curation, and visualization. C.Z. contributed to software, methodology, investigation, data curation, and visualization. P.F. contributed to conceptualization, supervision, and funding acquisition. D.E. contributed to conceptualization, supervision, and funding acquisition. All authors contributed to the writing of the manuscript.

Acknowledgments

P.F. acknowledges support by the Federal Ministry of Education and Research (BMBF) under Grant No. 01DM21001B (German-Canadian Materials Acceleration Center). P.F. acknowledges funding from the Klaus Tschira Stiftung gGmbH (SIMPLAIX project 1). P.K. acknowledges the computational resources and services used in part of work were provided by the VSC (Flemish Supercomputer Center), funded by the FWO and the Flemish Government, department EWI. The authors gratefully acknowledge the computing time provided on the high-performance computer HoreKa by the National High-Performance Computing Center at KIT (NHR@KIT). This center is jointly supported by the Federal Ministry of Education and Research and the Ministry of Science, Research and the Arts of Baden-Württemberg, as part of the National High-Performance Computing (NHR) joint funding program. HoreKa is partly funded by the German Research Foundation (DFG). D.E. acknowledges FWO (project number G022324N) for financial support.

Conflicts of Interest

The authors declare no conflicts of interest.

Data Availability Statement

The code of ML-NAMD is integrated with the parallel active learning library [63] developed by Zhou et al., and is available through the open-source repository on GitHub for continuous development, also by the community: https://github.com/aimat-lab/PAL (DOI: 10.5281/zenodo.15658962). The version of the code employed for this study is version 2.1.1. The NAMD and ML-NAMD trajectories data collected in this work can be found at Zenodo: https://doi.org/10.5281/zenodo.20655928 (DOI: 10.5281/zenodo.20655928).

References

1. C. W. Tang and S. A. VanSlyke, "Organic Electroluminescent Diodes," *Applied Physics Letters* 51, no. 12 (1987): 913–915.

2. J. H. Burroughes, D. D. Bradley, A. Brown, et al., "Light-Emitting Diodes Based on Conjugated Polymers," *Nature* 347, no. 6293 (1990): 539–541.

3. G. Hong, X. Gan, C. Leonhardt, et al., "A Brief History of OLEDs–Emitter Development and Industry Milestones," *Advanced Materials* 33, no. 9 (2021): 2005630.

4. R. Mertens, "The OLED Handbook: A Guide to OLED Technology, Industry & Market. 2015 Edition," *Ron Mertens, Herzelia, Israel* (2015).

5. D. J. Gaspar and E. Polikarpov, *OLED Fundamentals: Materials, Devices, and Processing of Organic Light-Emitting Diodes* (CRC press, 2015).

6. M. Baldo, S. Lamansky, P. Burrows, M. Thompson, and S. Forrest, "Very High-Efficiency Green Organic Light-Emitting Devices Based on Electrophosphorescence," *Applied Physics Letters* 75, no. 1 (1999): 4–6.

7. H. Uoyama, K. Goushi, K. Shizu, H. Nomura, and C. Adachi, "Highly Efficient Organic Light-Emitting Diodes From Delayed Fluorescence," *Nature* 492, no. 7428 (2012): 234–238.

8. H. Nakanotani, T. Higuchi, T. Furukawa et al., "High-Efficiency Organic Light-Emitting Diodes With Fluorescent Emitters," *Nature Communications* 5, no. 1 (2014): 4016.

9. H. Yersin, L. Mataranga-Popa, R. Czerwieniec, and Y. Dovbii, "Design of a New Mechanism Beyond Thermally Activated Delayed Fluorescence Toward Fourth Generation Organic Light Emitting Diodes," *Chemistry of Materials* 31, no. 16 (2019): 6110–6116.

10. N. Aizawa, Y.-J. Pu, Y. Harabuchi et al., "Delayed Fluorescence From Inverted Singlet and Triplet Excited States," *Nature* 609, no. 7927 (2022): 502–506.

11. S.-J. Zou, Y. Shen, F.-M. Xie, J.-D. Chen, Y.-Q. Li, and J.-X. Tang, "Recent Advances in Organic Light-Emitting Diodes: Toward Smart Lighting and Displays," *Materials Chemistry Frontiers* 4, no. 3 (2020): 788–820.

12. J. Song, H. Lee, E. G. Jeong, K. C. Choi, and S. Yoo, "Organic Light-Emitting Diodes: Pushing Toward the Limits and Beyond," *Advanced Materials* 32, no. 35 (2020): 1907539.

13. S. M. K. A. Naqvi, M. F. Baig, T. Farid, et al., "Unraveling Degradation Processes and Strategies for Enhancing Reliability in Organic Light-Emitting Diodes," *Nanomaterials* 13, no. 23 (2023): 3020.

14. A. S. Sandanayaka, T. Matsushima, and C. Adachi, "Degradation Mechanisms of Organic Light-Emitting Diodes Based on Thermally Activated Delayed Fluorescence Molecules," *The Journal of Physical Chemistry C* 119, no. 42 (2015): 23845–23851.

15. D. Wang, C. Cheng, T. Tsuboi, and Q. Zhang, "Degradation Mechanisms in Blue Organic Light-Emitting Diodes," *CCS Chemistry* 2, no. 4 (2020): 1278–1296.

16. S. Schmidbauer, A. Hohenleutner, and B. König, "Chemical Degradation in Organic Light-Emitting Devices: Mechanisms and Implications

25130390, 2026, 10, Downloaded from https://advanced.onlinelibrary.wiley.com/doi/10.1002/adts.70584 by Karlsruher Institut Fur Technologie, Wiley Online Library on [02/11/2026]. See the Terms and Conditions (https://onlinelibrary.wiley.com/terms-and-conditions) on Wiley Online Library for rules of use; OA articles are governed by the applicable Creative Commons License

for the Design of New Materials," *Advanced Materials* 25, no. 15 (2013): 2114–2129.

17. S. Scholz, D. Kondakov, B. Lussem, and K. Leo, "Degradation Mechanisms and Reactions in Organic Light-Emitting Devices," *Chemical Reviews* 115, no. 16 (2015): 8449–8503.

18. D. Jacquemin and D. Escudero, "The Short Device Lifetimes of Blue PhOLEDs: Insights Into the Photostability of Blue Ir (III) Complexes," *Chemical Science* 8, no. 11 (2017): 7844–7850.

19. S. S. Zumdahl, S. A. Zumdahl, and D. J. DeCoste, *Chemistry* (Cengage Learning, 2016).

20. C. Murawski, K. Leo, and M. C. Gather, "Efficiency Roll-Off in Organic Light-Emitting Diodes," *Advanced Materials* 25, no. 47 (2013): 6801–6827.

21. M. A. Baldo, C. Adachi, and S. R. Forrest, "Transient Analysis of Organic Electrophosphorescence. II. Transient Analysis of Triplet-Triplet Annihilation," *Physical Review B* 62, no. 16 (2000): 10967.

22. A. Y. Freidzon, A. A. Safonov, A. A. Bagaturyants et al., "Predicting the Operational Stability of Phosphorescent OLED Host Molecules From First Principles: A Case Study," *The Journal of Physical Chemistry C* 121, no. 40 (2017): 22422–22433.

23. H. Li, M. Hong, A. Scarpaci et al., "Chemical Stabilities of the Lowest Triplet State in Aryl Sulfones and Aryl Phosphine Oxides Relevant to Oled Applications," *Chemistry of Materials* 31, no. 5 (2019): 1507–1519.

24. P. Hohenberg and W. Kohn, "Inhomogeneous Electron Gas," *Physical Review* 136, no. 3B (1964): B864.

25. W. Kohn and L. J. Sham, "Self-Consistent Equations Including Exchange and Correlation Effects," *Physical Review* 140, no. 4A (1965): A1133.

26. C. Lee, W. Yang, and R. G. Parr, "Development of the Colle-Salvetti Correlation-Energy Formula Into a Functional of the Electron Density," *Physical Review B* 37, no. 2 (1988): 785.

27. A. D. Becke, "Density-Functional Thermochemistry. I. The Effect of the Exchange-Only Gradient Correction," *The Journal of Chemical Physics* 96, no. 3 (1992): 2155–2160.

28. A. D. Becke, "Density-Functional Thermochemistry. III. The Role of Exact Exchange," *The Journal of Chemical Physics* 98, no. 7 (1993): 5648–5652.

29. W. J. Hehre, R. Ditchfield, and J. A. Pople, "Self–Consistent Molecular Orbital Methods. XII. Further Extensions of Gaussian–Type Basis Sets for Use in Molecular Orbital Studies of Organic Molecules," *The Journal of Chemical Physics* 56, no. 5 (1972): 2257–2261.

30. P. C. Hariharan and J. A. Pople, "The Influence of Polarization Functions on Molecular orbital Hydrogenation Energies," *Theoretica Chimica acta* 28, no. 3 (1973): 213–222.

31. E. Runge and E. K. Gross, "Density-Functional Theory for Time-Dependent Systems," *Physical Review Letters* 52, no. 12 (1984): 997.

32. M. E. Casida, "Time-Dependent Density Functional Response Theory for Molecules," in *Recent Advances In Density Functional Methods: (Part I)* (World Scientific, 1995), 155–192.

33. M. A. Marques and E. K. Gross, "Time-Dependent Density Functional Theory," in *A Primer in Density Functional Theory* (Springer, 2003), 144–184.

34. A. E. Gross, J. Dobson, and M. Petersilka, "Density Functional Theory of Time-Dependent Phenomena," in *Density Functional Theory II: Relativistic and Time Dependent Extensions* (Springer, 2005), 81–172.

35. M. J. Frisch, G. W. Trucks, H. B. Schlegel, et al., "Gaussian 16," Revision A.03 (Gaussian, Inc., Wallingford, CT, 2016).

36. S. Grimme, "Semiempirical Hybrid Density Functional With Perturbative Second-Order Correlation," *The Journal of Chemical Physics* 124, no. 3 (2006): 034–108.

37. M. Wormit, D. R. Rehn, P. H. Harbach et al., "Investigating Excited Electronic States Using the Algebraic Diagrammatic Construction (ADC) Approach of the Polarisation Propagator," *Molecular Physics* 112, no. 5-6 (2014): 774–784.

38. J. Schirmer, "Beyond the Random-Phase Approximation: A New Approximation Scheme for the Polarization Propagator," *Physical Review A* 26, no. 5 (1982): 2395.

39. J. Schirmer and A. B. Trofimov, "Intermediate State Representation Approach to Physical Properties of Electronically Excited Molecules," *The Journal of Chemical Physics* 120, no. 24 (2004): 11449–11464.

40. A. B. Trofimov and J. Schirmer, "An Efficient Polarization Propagator Approach to Valence Electron Excitation Spectra," *Journal of Physics B: Atomic, Molecular and Optical Physics* 28, no. 12 (1995): 2299–2324.

41. F. Weigend and R. Ahlrichs, "Balanced Basis Sets of Split Valence, Triple Zeta Valence and Quadruple Zeta Valence Quality for H to Rn: Design and Assessment of Accuracy," *Physical Chemistry Chemical Physics* 7, no. 18 (2005): 3297–3305.

42. F. Furche, R. Ahlrichs, C. Hättig, W. Klopper, M. Sierka, and F. Weigend, "Turbomole," *Wiley Interdisciplinary Reviews: Computational Molecular Science* 4, no. 2 (2014): 91–100.

43. R. Crespo-Otero and M. Barbatti, "Recent Advances and Perspectives on Nonadiabatic Mixed Quantum–Classical Dynamics," *Chemical Reviews* 118, no. 15 (2018): 7026–7068.

44. A. Jain and A. Sindhu, "Pedagogical Overview of the Fewest Switches Surface Hopping Method," *ACS Omega* 7, no. 50 (2022): 45810–45824.

45. M. Barbatti and R. Crespo-Otero, "Surface Hopping Dynamics With DFT Excited States," *Density-Functional Methods for Excited States, Topics in Current Chemistry* 368 (2016): 415–444.

46. J. C. Tully, "Molecular Dynamics With Electronic Transitions," *The Journal of Chemical Physics* 93, no. 2 (1990): 1061–1071.

47. M. Barbatti, M. Bondanza, R. Crespo-Otero et al., "Newton-X Platform: New Software Developments for Surface Hopping and Nuclear Ensembles," *Journal of Chemical Theory and Computation* 18, no. 11 (2022): 6851–6865, https://doi.org/10.1021/acs.jctc.2c00804.

48. S. Hammes-Schiffer and J. C. Tully, "Proton Transfer in Solution: Molecular Dynamics With Quantum Transitions," *The Journal of Chemical Physics* 101, no. 6 (1994): 4657–4667, https://doi.org/10.1063/1.467455.

49. Z. Wang, C. Wu, and W. Liu, "NAC-TDDFT: Time-Dependent Density Functional Theory for Nonadiabatic Couplings," *Accounts of Chemical Research* 54, no. 17 (2021): 3288–3297, https://doi.org/10.1021/acs.accounts.1c00312.

50. M. Barbatti, M. Bondanza, R. Crespo-Otero et al., "Newton-X Platform: New Software Developments for Surface Hopping and Nuclear Ensembles," *Journal of Chemical Theory and Computation* 18, no. 11 (2022): 6851–6865.

51. J. Westermayr, M. Gastegger, M. F. Menger, S. Mai, L. González, and P. Marquetand, "Machine Learning Enables Long Time Scale Molecular Photodynamics Simulations," *Chemical Science* 10, no. 35 (2019): 8100–8107.

52. J. Li, P. Reiser, B. R. Boswell et al., "Automatic Discovery of Photoisomerization Mechanisms With Nanosecond Machine Learning Photodynamics Simulations," *Chemical Science* 12 (2021): 5302–5314, https://doi.org/10.1039/D0SC05610C.

53. L. Yu, C. Xu, Y. Lei, C. Zhu, and Z. Wen, "Trajectory-Based Nonadiabatic Molecular Dynamics Without Calculating Nonadiabatic Coupling in the Avoided Crossing Case: Trans - Cis Photoisomerization in Azobenzene," *Physical Chemistry Chemical Physics* 16 (2014): 25883–25895, https://doi.org/10.1039/C4CP03498H.

54. S. Axelrod, E. Shakhnovich, and R. Gómez-Bombarelli, "Excited State Non-Adiabatic Dynamics of Large Photoswitchable Molecules Using a Chemically Transferable Machine Learning Potential," *Nature Communications* 13, no. 1 (2022): 3440.

25130390, 2026, 10, Downloaded from https://advanced.onlinelibrary.wiley.com/doi/10.1002/adts.70584 by Karlsruher Institut Fur Technologie, Wiley Online Library on [02/11/2026]. See the Terms and Conditions (https://onlinelibrary.wiley.com/terms-and-conditions) on Wiley Online Library for rules of use; OA articles are governed by the applicable Creative Commons License

55. D. Kasemann, R. Brückner, H. Fröb, and K. Leo, "Organic Light-Emitting Diodes Under High Currents Explored by Transient Electroluminescence on the Nanosecond Scale," *Physical Review B* 84, no. 11 (2011): 115208.

56. E. Tankeleviciute, I. D. Samuel, and E. Zysman-Colman, "The Blue Problem: OLED Stability and Degradation Mechanisms," *The Journal of Physical Chemistry Letters* 15, no. 4 (2024): 1034–1047.

57. M. Tanaka, R. Nagata, H. Nakanotani, and C. Adachi, "Understanding Degradation of Organic Light-Emitting Diodes From Magnetic Field Effects," *Communications Materials* 1, no. 1 (2020): 18.

58. N. Nakashima and K. Yoshihara, "Role of Hot Molecules Formed by Internal Conversion in UV Single-Photon and Multiphoton Chemistry," *The Journal of Physical Chemistry* 93, no. 23 (1989): 7763–7771.

59. D. Y. Kondakov, "Triplet–Triplet Annihilation in Highly Efficient Fluorescent Organic Light-Emitting Diodes: Current State and Future Outlook," *Philosophical Transactions of the Royal Society A: Mathematical, Physical and Engineering Sciences* 373, no. 2044 (2015): 20140321.

60. H.-W. Lee, "Wigner Trajectories of a Gaussian Wave Packet Perturbed by a Weak Potential," *Foundations of Physics* 22, no. 8 (1992): 995–1010.

61. A. Prlj, J. T. Taylor, J. Janoš et al., "Best Practices for Nonadiabatic Molecular Dynamics Simulations," *arXiv preprint arXiv:2508.05263* (2025).

62. P. O. Dral, M. Barbatti, and W. Thiel, "Nonadiabatic Excited-State Dynamics With Machine Learning," *The Journal of Physical Chemistry Letters* 9, no. 19 (2018): 5660–5663.

63. C. Zhou, M. Neubert, Y. Koide et al., "PAL – Parallel Active Learning for Machine-Learned Potentials," *Digital Discovery* 4 (2025): 1901–1911, https://doi.org/10.1039/D5DD00073D.

Supporting Information

Additional supporting information can be found online in the Supporting Information section.

Supporting File: adts70584-sup-0001-SuppMat.pdf.

25130390, 2026, 10, Downloaded from https://advanced.onlinelibrary.wiley.com/doi/10.1002/adts.70584 by Karlsruher Institut Fur Technologie, Wiley Online Library on [02/11/2026]. See the Terms and Conditions (https://onlinelibrary.wiley.com/terms-and-conditions) on Wiley Online Library for rules of use; OA articles are governed by the applicable Creative Commons License